J. Fluid Mech. (1971), *vol.* 48, *part* 3, *pp.* 429–461
Printed in Great Britain

Magnetohydrodynamic duct flow in a uniform transverse magnetic field of arbitrary orientation

By C. J. N. ALTY
School of Engineering Science, The University of Warwick

(Received 22 August 1968 and in revised form 19 March 1971)

The paper presents an approximate analysis for high Hartmann number of the flow of an electrically conducting, incompressible fluid in a duct of square cross-section, having one pair of opposite walls insulating, and the other pair perfectly conducting and inclined at arbitrary orientation to a uniform transverse magnetic field. The flow is considered to be either pressure-driven with the two perfectly conducting electrodes short-circuited together or electrically driven by a potential difference applied between these electrodes in the absence of axial pressure gradient. The paper describes experiments on the pressure-driven, short-circuited case using mercury in copper ducts to investigate the variation of the streamwise pressure gradient and of the potential distribution along one insulating wall with orientation, magnetic field and flow rate.

At general orientations the analysis suggests and the experiments confirm the existence of regions of stationary fluid in the corners of the duct, together with viscous shear layers parallel to the magnetic field. For the case in which the electrodes are parallel to the magnetic field the experimental results for the pressure gradient, but not those for the potential distribution, agree reasonably well with Hunt & Stewartson's (1965) asymptotic solution. Both pressure gradient and potential results agree closely with the analysis by Hunt (1965) of the case in which the electrodes are perpendicular to the magnetic field.

1. Introduction

The development of magnetohydrodynamic devices such as power generators, pumps and flowmeters with both conducting and non-conducting walls has led to considerable interest in the flow of fluids in rectangular ducts in the presence of transverse magnetic fields. The general practical situation is so intractable that solutions have first been sought for cases of the fully developed, laminar, incompressible flow of uniformly conducting fluids in ducts of constant cross-section.

Hunt & Stewartson (1965) analyzed the flow in a rectangular duct having perfectly conducting walls parallel to the magnetic field and insulating walls perpendicular to the field, which is the geometry of greatest technological interest. The flow is driven by either an axial pressure gradient or an applied potential difference between the perfectly conducting walls, or both. They showed that at high Hartmann numbers M, the flow in a duct of width $2a$ in the field direction

consists of a central core moving with uniform velocity, together with Hartmann boundary layers of thickness of order a/M on the walls perpendicular to the field, and boundary layers of thickness of order $a/M^{\frac{1}{2}}$ in which the velocity falls monotonically on the walls parallel to the field. The form of the velocity distribution is independent of the external electrical circuit, if any.

Hunt (1965) analyzed the case in which the above duct has been rotated through 90° relative to the field direction. At high Hartmann numbers he again found Hartmann boundary layers on the walls perpendicular to the field, flanking a central core of uniform velocity v_c. On the walls parallel to the field he found boundary layers of thickness of order $a/M^{\frac{1}{2}}$, within which the velocity profile is approximately of the form of exponentially damped sine waves with peak velocities of order Mv_c.

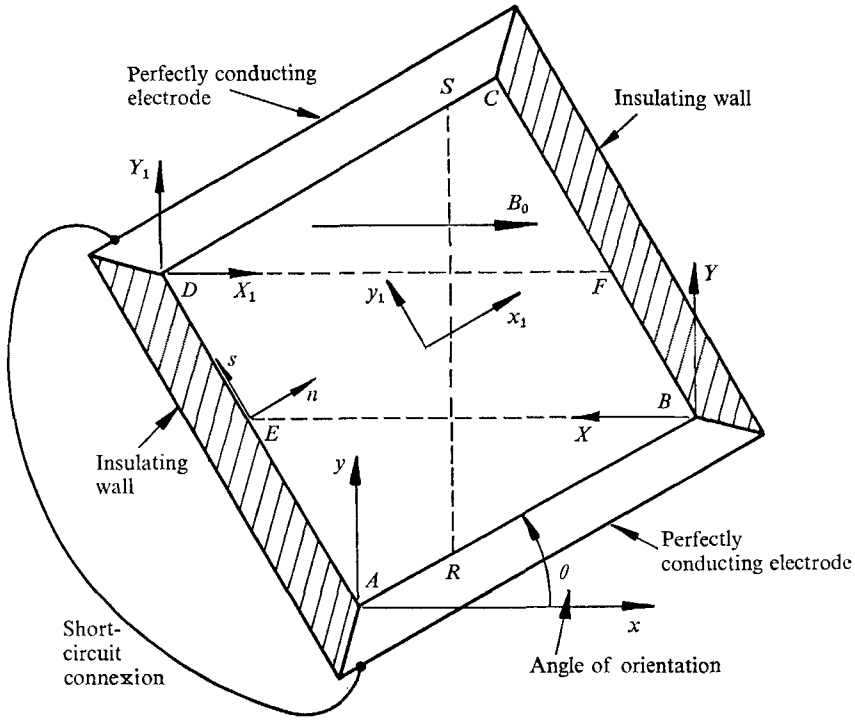

FIGURE 1. Cross-section of square duct with walls of mixed conductivities at arbitrary orientation to a transverse magnetic field. The z axis is directed out of the page.

$$AB = BC = 2a.$$

The present work is concerned to bridge the gap between these two markedly different situations by considering the flow in a duct of uniform, square cross-section with one pair of opposite walls insulating and the other pair perfectly conducting and at arbitrary orientation to the transverse magnetic field, as in figure 1. Preliminary analysis of the situation for high Hartmann numbers by Shercliff (private communication) led to the surprising prediction that, at general orientations θ of the perfectly conducting walls to the magnetic field, the

fluid would be at rest in the two triangles ABE and CDF, cut off by lines through the corners of the duct parallel to the field. Shercliff also showed that for pressure-driven flow with the two perfectly conducting walls short-circuited together at orientations below 45° the pressure gradient for a given flow rate and field strength would vary as $\cos^2\theta$.

This paper presents further approximate theoretical analysis of the situation for orientations above and below 45° for pressure-driven short-circuited flow and for electrically driven flow with no axial pressure gradient. It is found that the vanishing of the fluid velocity in the triangles is a freak property of ducts which have right-angled corners in the triangles. The flow in the central parallelogram region is found to consist of forms of skewed Hartmann flow, separated from the stationary régimes in the triangles by thin viscous layers or wakes of thickness of order $a/M^{\frac{1}{2}}$ lying parallel to the magnetic field.

For orientations below 45° the velocity in each layer is found to vary in approximately the error function manner. Solutions of this type have been found by several workers in comparable configurations. Hasimoto (1960) considered the case of the steady motion in its own plane and parallel to its edge of a semi-infinite perfectly conducting flat plate in a conducting fluid in the presence of a uniform transverse magnetic field. At high Hartmann numbers he found approximately parabolic wakes, aligned with the magnetic field and emanating from the edge of the plate, within which the fluid velocity and the induced magnetic field vary in the error function manner. Outside the wakes, the fluid in the half-space containing the plate moves at the same velocity as the plate, while the fluid in the other half-space is at rest.

Todd (1967) found similar wakes in the flow at high Hartmann numbers along the annular channel between two non-conducting circular cylinders, whether concentric or not, in the presence of a uniform transverse magnetic field. In that case the parabolic wakes are centred on the magnetic field lines which are tangential to the inner cylinder.

Hunt & Williams (1968) discussed previous work on the occurrence of layers or wakes aligned with magnetic fields. They extended the work by considering the electrically driven flow of a fluid between two parallel non-conducting planes fitted with a pair of parallel line electrodes in the presence of a magnetic field perpendicular to the planes. For large Hartmann numbers M for the cases in which the electrodes were opposite one another or offset they found thin layers, of thickness of order $a/M^{\frac{1}{2}}$ where $2a$ was the separation of the planes, extending from the electrodes in the direction of the magnetic field, within which the velocity varied in the error function manner. Hunt & Williams' result for the case of offset electrodes closely resembles the solution found in §4 of the present paper for electrically driven flow for orientations θ of less than 45°.

For orientations above 45° there are found to be discontinuities across the layers both in the velocity and in the component of electric field parallel to the applied magnetic field. Situations involving similar discontinuities have been discussed by several workers. The theoretical studies of Yakubenko (1963), Moffatt (1964), and Waechter (1968) have been reviewed by Hunt & Williams (1968). Moffatt pointed out that a discontinuity across a layer in the component

of electric field parallel to the layer would give rise to large electric fields normal to the layer. As large currents in that direction do not occur, there must be large opposing induced e.m.f.s $\mathbf{v} \times \mathbf{B}$, and these in turn call for large fluid velocities within the layer. Hunt & Stewartson (1969) obtained a complete asymptotic solution to the problem, discussed earlier by Hunt & Malcolm (1968), of the electrically driven flow of a conducting fluid between two circular electrodes set opposite one another in insulating planes, with a uniform magnetic field applied perpendicular to the planes. At high Hartmann numbers they predicted the existence of thin circumferential shear layers joining the rims of the electrodes, within which high fluid velocities would occur. Their theoretical results for the potential and velocity distributions within the shear layers agreed closely with the experimental results of Hunt & Malcolm (1968) and Malcolm (1968), which convincingly demonstrated the existence of these high velocity layers.

The paper describes how the theory was tested in experiments at Hartmann numbers greater than 100 on the pressure-driven flow of mercury in copper ducts with the pair of highly conducting walls short-circuited together. Measurements were made of the variation with orientation, field strength and flow rate of the streamwise pressure gradient and the electric potential distribution along one of the insulating walls. The results for pressure gradient were consistently higher than anticipated and suggested a relative correction of order M^{-1}, which is not understood. The potential results, except for anomalies at zero orientation, agreed closely with the theoretical predictions, and afford convincing evidence that the mercury in the two triangular regions was at rest. A detailed description of the work is given in the author's thesis (Alty 1966).

The work described in this paper was mentioned in a lecture by Shercliff (1967). Subsequently, Kulikovskii (1968) gave a general discussion of such flows at high Hartmann numbers. He indicated how discontinuities in the boundary conditions associated with such a flow lead to the division of the core into distinct regions separated by thin viscous layers, parallel to the magnetic field, across which discontinuities in various properties may occur.

2. The governing equations

We consider the steady rectilinear flow of an incompressible and non-magnetic fluid of uniform conductivity σ, viscosity η and density ρ in a straight duct whose cross-section is shown in figure 1, together with the co-ordinate axes used. The perfectly conducting electrodes are inclined at an angle θ to a uniform transverse applied magnetic field of flux density B_0. The flow is either pressure-driven with the two electrodes short-circuited together as in figure 1, or electrically driven by a potential difference applied between the electrodes. There is no variation in the z direction in the geometry of the duct, in the conductivity of the walls or in the transverse magnetic field, and the external circuit connected between the electrodes is continuous in the z direction. The flow is fully developed and all quantities (except pressure in the pressure-driven case) are independent of z. It follows that the pressure gradient $\partial p/\partial z$, if any, is constant throughout the cross-section of the duct and that current flow is confined to x, y planes.

From Shercliff (1965), the equations governing the flow take the following form in rationalized M.K.S. units:

$$j_x = \sigma E_x; \quad j_y = \sigma(E_y + v_z B_0), \tag{2.1}$$

$$0 = \eta\left(\frac{\partial^2 v_z}{\partial x^2} + \frac{\partial^2 v_z}{\partial y^2}\right) - j_y B_0 - \frac{\partial p}{\partial z}, \tag{2.2}$$

$$j_x = \frac{1}{\mu}\frac{\partial B_z}{\partial y}; \quad j_y = -\frac{1}{\mu}\frac{\partial B_z}{\partial x}, \tag{2.3}$$

where j_x and j_y are the components of the current density $\mathbf{j}$; E_x and E_y are the components of electric field $\mathbf{E}$; v_z is the velocity of the fluid and μ is the permeability of free space. It follows that

$$\frac{B_0}{\mu}\frac{\partial B_z}{\partial x} + \eta\left(\frac{\partial^2 v_z}{\partial x^2} + \frac{\partial^2 v_z}{\partial y^2}\right) = \frac{\partial p}{\partial z}, \tag{2.4}$$

and that

$$B_0\frac{\partial v_z}{\partial x} + \frac{1}{\mu\sigma}\left(\frac{\partial^2 B_z}{\partial x^2} + \frac{\partial^2 B_z}{\partial y^2}\right) = 0. \tag{2.5}$$

We also have the equations

$$\frac{\partial j_x}{\partial x} + \frac{\partial j_y}{\partial y} = 0; \quad \frac{\partial E_y}{\partial x} - \frac{\partial E_x}{\partial y} = 0. \tag{2.6}$$

The Hartmann number M, based on the half-width a of the duct, is defined by

$$M = B_0 a(\sigma/\eta)^{\frac{1}{2}}. \tag{2.7}$$

3. Orientations between zero and 45°: pressure-driven short-circuited case

Shercliff (private communication) made a preliminary analysis of the pressure-driven short-circuited case, shown in figure 1, for high Hartmann numbers. He considered the flow to consist of core regions, within which viscosity was negligible, together with vanishingly thin boundary layers on the walls. Shercliff argued that, as in the case of a square duct all of whose walls are perfectly conducting, the currents circulating between the fluid and the walls would be so great that the current content of the boundary layers on the walls would be negligibly small in comparison. This implies that at the edge of the core region near to each insulating wall the direction of current flow is parallel to the wall, that is $j_x/j_y = -\tan\theta$, and that at the edge of the core near to each perfectly conducting electrode the electric field is normal to the electrode, that is $E_x/E_y = -\tan\theta$.

Within the core viscous forces are negligible, and so from (2.2) j_y in the core is uniform at the value $(1/B_0)(-\partial p/\partial z)$. It follows that at the edges of the core adjacent to the insulating walls j_x also is uniform, and that, in view of (2.6), j_x is independent of x in the core regions. From these results it follows that throughout the core regions j_x is uniform and the total current density $\mathbf{j}$ is of magnitude $(\sec\theta/B_0)(-\partial p/\partial z)$ parallel to the insulating walls.

A similar argument relates to the electric field in the core. From (2.1) E_x is uniform in the core regions. It follows that E_y is uniform at the edges of the core adjacent to the perfectly conducting electrodes, and that, in view of (2.6), E_y in the core is independent of x. Consequently, throughout the core regions in the triangles ABE and CDF of figure 1 E_y is uniform and the total electric field $\mathbf{E}$ is normal to the electrodes, and therefore, for a duct of square cross-section, parallel to the insulating walls. In the Ohm's law equation

$$\mathbf{j} = \sigma(\mathbf{E} + \mathbf{v} \times \mathbf{B}) \tag{3.1}$$

for the triangles ABE and CDF, both $\mathbf{j}$ and $\mathbf{E}$ are parallel to the insulating walls, whereas $\mathbf{v} \times \mathbf{B}$, if non-zero, is in the y direction. It follows that $v_z = 0$ in the triangles and that the fluid there is at rest. This is a result of the fact that the angles at A and C are 90°.

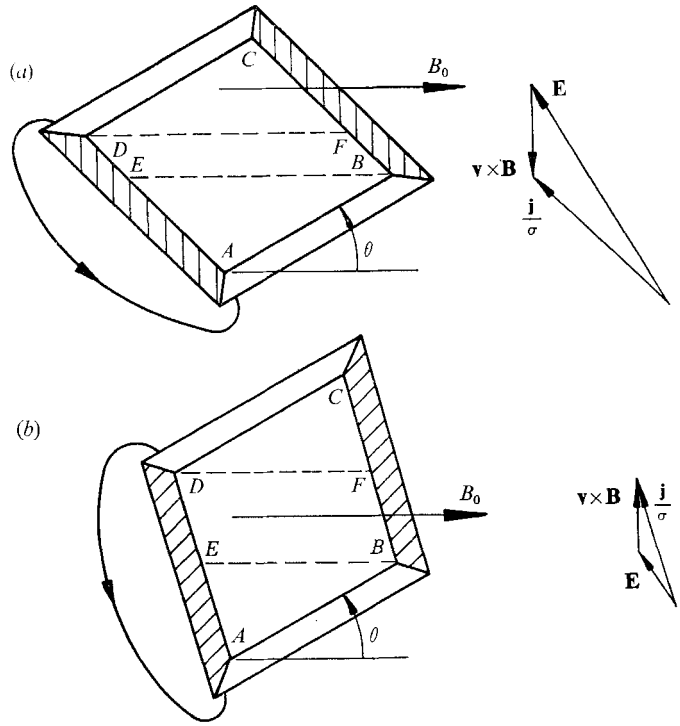

FIGURE 2. Cross-sections of rhombic ducts with vector diagrams for Ohm's law in triangles ABE and CDF; (a) angle $BAD > 90°$, $v_z < 0$ in triangles; (b) angle $BAD < 90°$, $v_z > 0$ in triangles.

In the case of ducts of non-square cross-section, such as the rhombic sections shown in figure 2, the current density $\mathbf{j}$ in the core in each of the triangles ABE and CDF is parallel to the adjacent insulating wall and the electric field $\mathbf{E}$ is normal to the electrode. The vector diagrams for (3.1) take the form shown, and the core velocities in the triangles are non-zero. The general result is that the core velocity in each triangular region is positive, zero or negative, depending on whether the corner angle is less than, equal to or greater than 90°. If the corner angle is

denoted by $(90-\phi)$, the core velocity in the triangle when the adjacent electrode makes an angle θ with the transverse field is given by

$$v_z = \frac{1}{B_0^2\sigma}\left(-\frac{\partial p}{\partial z}\right)\frac{\sec\theta\,\mathrm{cosec}\,\theta\tan\phi}{1+\tan\theta\tan\phi}. \tag{3.2}$$

When $\phi = \theta$, so that the insulating wall is perpendicular to the magnetic field, **E** is zero and the core velocity in the triangle is $(1/B_0^2\sigma)\,(-\partial p/\partial z)$, as in an all-perfectly conducting duct.

In the square duct of figure 1, motion is confined to the region $EBFD$, where we expect that the flow consists of a core, within which viscous forces are negligible, surrounded by boundary layers along DE and FB and viscous shear layers along the lines BE and DF. Shercliff noted that within the core of region $EBFD$ the velocity is independent of x. This is clear from the y component of the Ohm's law equation, $j_y/\sigma = E_y + v_z B_0$, since in the core regions j_y is uniform and E_y is independent of x. This result is an example of the tendency of a magnetic field to suppress vorticity perpendicular to itself.

To deduce the relationship, first derived by Shercliff, between pressure gradient and flow rate we set up x_1 and y_1 axes as shown in figure 1 and integrate the terms of the y_1 component of the Ohm's law equation with respect to x_1 and y_1 over the entire cross-section of the duct.

$$\int_{-a}^{a}\int_{-a}^{a}(j_{y_1}/\sigma)\,dx_1 dy_1 = \int_{-a}^{a}\int_{-a}^{a}E_{y_1}dx_1 dy_1 + B_0\cos\theta\int_{-a}^{a}\int_{-a}^{a}v_z dx_1 dy_1. \tag{3.3}$$

By virtue of the short-circuit connexion

$$\int_{-a}^{a}E_{y_1}dy_1 = 0$$

for all x_1. Throughout the core regions $j_{y_1} = (\sec\theta/B_0)\,(-\partial p/\partial z)$. The volumetric flow rate Q is given by

$$Q = \int_{-a}^{a}\int_{-a}^{a}v_z dx_1 dy_1.$$

On substituting these results into (3.3) and neglecting errors due to boundary layers, we obtain Shercliff's approximate relation

$$-\frac{\partial p}{\partial z} = \frac{B_0^2\sigma Q\cos^2\theta}{4a^2} = B_0^2\sigma v_0\cos^2\theta, \tag{3.4}$$

where v_0 is the mean velocity, $Q/4a^2$. Shercliff pointed out that as θ approaches 45° the parallelogram region $EBFD$, which carries the flow, shrinks towards zero area while the flow rate remains finite. That is, the velocity distribution in the y direction takes the form of a delta function, in this inviscid approximation.

Except close to the lines BE and DF, the flow in the parallelogram region $EBFD$ is the same as Hartmann flow between infinite plane insulating walls parallel to DE, with the same normal transverse magnetic field $B_0\cos\theta$ and with an appropriate constraint on the electric field. This may be seen from a consideration of Shercliff's (1953) compound variables

$$v\,(=v_z + B_z/\mu(\sigma\eta)^{\frac{1}{2}}) \quad \text{and} \quad w\,(=v_z - B_z/\mu(\sigma\eta)^{\frac{1}{2}}).$$

For high Hartmann numbers, v (and likewise w) is determined at one wall, varies (if at all) linearly with distance from it in the field direction, and has a boundary layer on the other wall. The effect of a discontinuity in the value of v on the wall without a boundary layer is that at a distance x from that wall in the field direction the disturbance extends a distance of order $x/M^{\frac{1}{2}}$ in the direction normal to the field. Assuming that the electric field changes abruptly on the lines BE and DF, we find that the velocity profile in the region $EBFD$ is given by

$$v_z = u\left\{1 - \frac{\cosh(M\cos\theta x_1/a)}{\cosh(M\cos\theta)}\right\}, \tag{3.5}$$

in which

$$u = \frac{-\partial p/\partial z}{B_0^2\sigma\cos\theta(\cos\theta - \sin\theta)}. \tag{3.6}$$

With $M\cos\theta$ large, a central core of uniform velocity u is flanked by skew Hartmann boundary layers of thickness of order $a/M\cos\theta$. As the orientation approaches 45°, the viscous regions in the vicinity of the lines BE and DF coalesce, the skew Hartmann region vanishes and the infinite velocity predicted by (3.6) at $\theta = 45°$ is avoided. The result (3.6) can alternatively be derived from Shercliff's expression (3.4), by ignoring the details of the flow in the viscous regions and simply dividing the flow rate by the area of $EBFD$.

If the flow deficit due to the skew Hartmann boundary layers is allowed for but possible errors due to the viscous layers centred on BE and DF are neglected, the volumetric flow rate Q through the duct is given by

$$Q = \frac{4a^2\sec^2\theta}{B_0^2\sigma}\left(-\frac{\partial p}{\partial z}\right)\left\{1 - \frac{1}{M\cos\theta}\right\}. \tag{3.7}$$

For the analysis of the flow in the neighbourhood of the lines BE and DF, the differential equations (2.4) and (2.5) are uncoupled and the relevant boundary conditions simplified by the substitutions

$$\left.\begin{aligned} V &= v_z + B_z/\mu(\sigma\eta)^{\frac{1}{2}} - [1/B_0(\sigma\eta)^{\frac{1}{2}}][-\partial p/\partial z][2a\sec\theta - (x + y\tan\theta)] + 2u, \\ W &= v_z - B_z/\mu(\sigma\eta)^{\frac{1}{2}} + [1/B_0(\sigma\eta)^{\frac{1}{2}}][-\partial p/\partial z][2a\sec\theta - (x + y\tan\theta)] - 2u. \end{aligned}\right\} \tag{3.8}$$

Assuming that for large Hartmann numbers the layers are thin, we may neglect $\partial^2/\partial x^2$ in comparison with $\partial^2/\partial y^2$. Then, in terms of the (X, Y) co-ordinates shown in figure 1, the equations for the layer centred on the line BE become

$$\frac{\partial^2 V}{\partial Y^2} - \frac{M}{a}\frac{\partial V}{\partial X} = 0; \quad \frac{\partial^2 W}{\partial Y^2} + \frac{M}{a}\frac{\partial W}{\partial X} = 0. \tag{3.9}$$

The following boundary conditions apply: in the triangle ABE, $V = W = 0$; in the core of region $EBFD$, $V = 2u$, $W = 0$; close to the corner B the conditions are obscure. A plausible solution is that within the layer W is constant at zero and V is given by

$$V = u(1 + \operatorname{erf} p), \tag{3.10}$$

where erf is the error function and $p = M^{\frac{1}{2}}Y/(4aX)^{\frac{1}{2}}$. The corresponding solutions for v_z and B_z in the layer centred on the line BE are

$$\left.\begin{aligned} v_z &= \tfrac{1}{2}u(1 + \operatorname{erf} p), \\ B_z &= \tfrac{1}{2}\mu u(\sigma\eta)^{\frac{1}{2}}(1 + \operatorname{erf} p) - 2\mu u(\sigma\eta)^{\frac{1}{2}} + (\mu/B_0)(-\partial p/\partial z) \\ &\qquad \times [2a\sec\theta - (x + y\tan\theta)]. \end{aligned}\right\} \tag{3.11}$$

As was mentioned in §1, this solution resembles the results obtained by Hasimoto (1960), Todd (1967) and Hunt & Williams (1968) for similar configurations. However, the error function solution is somewhat suspect in the present case on account of the obscurity of the conditions in the corners B and D, which affect the régime, not only locally, but throughout the viscous layers.

Since $\operatorname{erf} 1{\cdot}38 = 0{\cdot}95$, the difference in velocity between a pair of points for which $p = \pm 1{\cdot}38$ is 95 % of the total velocity change across the layer. Thus we may regard the locus $p = \pm 1{\cdot}38$, which is a parabola centred on BE with its vertex at B, as the boundary of the layer. The analysis of the flow in the vicinity of the line DF is similar: a parabolic layer, within which v_z varies in approximately the error function manner, emanates from D.

In the present solution E_y is antisymmetric about the centreline of each of the layers. It follows that the expression (3.6) for the core velocity u in the parallelogram region, found earlier on the assumption that the electric field changes abruptly across the lines BE and DF, requires no modification on account of the finite thickness of the layers. Similarly, in view of the antisymmetry of the error function, the expression (3.7) for the total volumetric flow rate through the duct requires no correction on these grounds.

It is possible to make an approximate analysis of the flow in the vicinity of points E and F of figure 1, where the skew Hartmann boundary layers and the error function layers coalesce. In terms of the (s, n) co-ordinates shown in figure 1, we find that in the vicinity of E

$$\left.\begin{aligned} v_z &= \tfrac{1}{2}u(1+\operatorname{erf} p)\,[1-\exp(-nM\cos\theta/a)], \\ B_z &= \tfrac{1}{2}\mu u(\sigma\eta)^{\frac{1}{2}}(1+\operatorname{erf} p)\,[1-\exp(-nM\cos\theta/a)] \\ &\quad -2\mu u(\sigma\eta)^{\frac{1}{2}} + (\mu/B_0)(-\partial p/\partial z)\,[2a\sec\theta-(x+y\tan\theta)]. \end{aligned}\right\} \tag{3.12}$$

Similar expressions may be derived for v_z and B_z in the neighbourhood of point F.

We may use (3.12) to derive the following expression for E_{y_1}, the electric field component in the direction ED, at the wall in the vicinity of point E:

$$E_{y_1} = (\sec\theta/B_0\sigma)(-\partial p/\partial z)\,[1-(1+\operatorname{erf} p_w)/2(1-\tan\theta)], \tag{3.13}$$

in which p_w is the value of p at a point on the wall. Equation (3.13) may be integrated to yield the potential distribution along the wall AD. The potential profile falls linearly from A to the vicinity of E, where its slope changes smoothly from negative to positive, and then rises linearly to D to satisfy the short-circuit condition.

Figure 3, drawn for the case of $\theta = 20°$ and $M = 200$, summarizes the solution obtained for the pressure-driven short-circuited case for orientations of less than 45°. It shows the velocity profile in the y direction through the mid-point of the duct and some approximate current flow lines. In the two zones 1 the fluid is at rest and there are no boundary layers on the walls. Zone 2 is the core of a region of skew Hartmann flow in which the fluid moves with the uniform velocity given by (3.6). In zones 1 and 2 current flows with uniform density parallel to the insulating walls, and the Lorentz force $\mathbf{j}\times\mathbf{B}$ balances the pressure gradient.

The two zones 3 are skew Hartmann boundary layers of thickness of order $a/M\cos\theta$ within which the velocity rises from zero at the walls to its uniform

value in zone 2. The current density lies in the directions DK and LB in the fluid at the walls, reverses within the boundary layers, and at the outer edges of the layers is identical with that in zone 2.

The two zones 4 are layers parallel to the applied magnetic field of thickness of order $a/M^{\frac{1}{2}}$, which spread parabolically from corners B and D but do not diffuse in the downstream direction. Within the layers the velocity increases in approximately the error function manner from zero in the two zones 1 to its uniform value in zone 2.

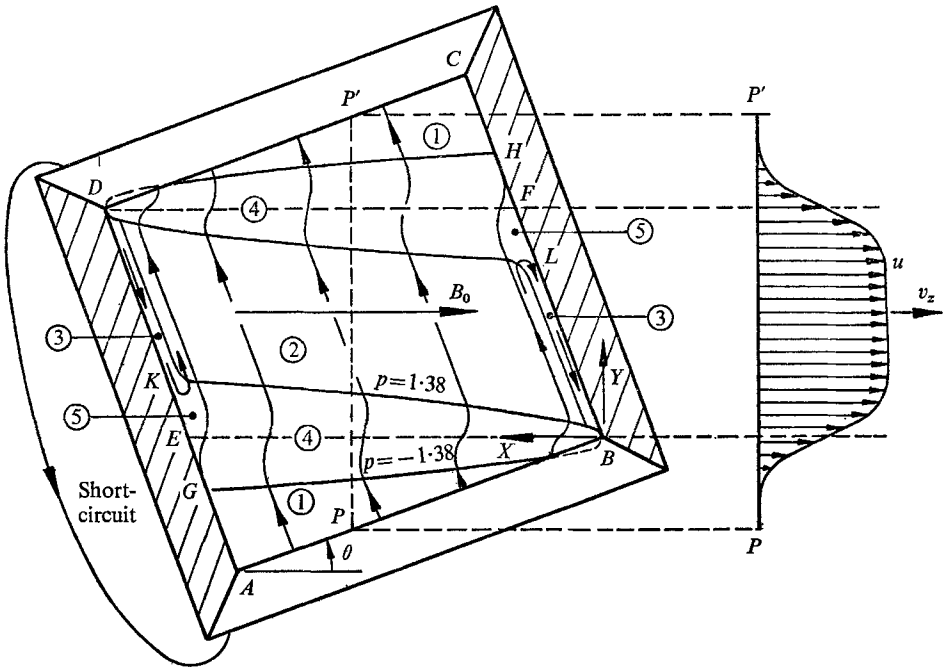

FIGURE 3. The form of the viscous layers parallel to the magnetic field, approximate current flow lines and a velocity profile for the pressure-driven short-circuited case for $\theta < 45°$ (drawn for the case of $\theta = 20°$ and $M = 200$). The thickness of the skew Hartmann boundary layers is exaggerated.

The two zones 5 are skew Hartmann boundary layers of varying strength. Their current contents and the velocity jumps across them increase from zero at G and H to the full values corresponding to the skew Hartmann boundary layers of zones 3 at K and L.

4. Orientations between zero and 45°: electrically driven case without axial pressure gradient

Analysis closely similar to that given in §3 may be developed for the case of a square duct with walls of mixed conductivities when the flow is electrically driven by a potential difference V applied between the electrodes, in the absence of an axial pressure gradient. Figure 4, which is drawn for the case $\theta = 20°$ and $M = 200$, summarizes the results and shows approximate current flow lines. The form of the

velocity distribution is found to be identical to that in the pressure-driven short-circuited case. The solution closely resembles that found theoretically by Hunt & Williams (1968) for electrically driven flow between offset parallel line electrodes set in infinite plane insulating walls in the presence of a transverse magnetic field.

In the two zones 1 the fluid is at rest, at uniform potential and current free. There are no viscous forces, Lorentz forces or pressure forces. Zone 2 is the core of a region of skew Hartmann flow in which the fluid moves with uniform velocity given by the equation

$$u = \frac{V}{2aB_0(\cos\theta - \sin\theta)}. \tag{4.1}$$

The electric field is perpendicular to the transverse magnetic field and is equal and opposite to the e.m.f. $\mathbf{v} \times \mathbf{B}$ due to motion, so that the zone is current free. All the terms of the Navier–Stokes equation are zero.

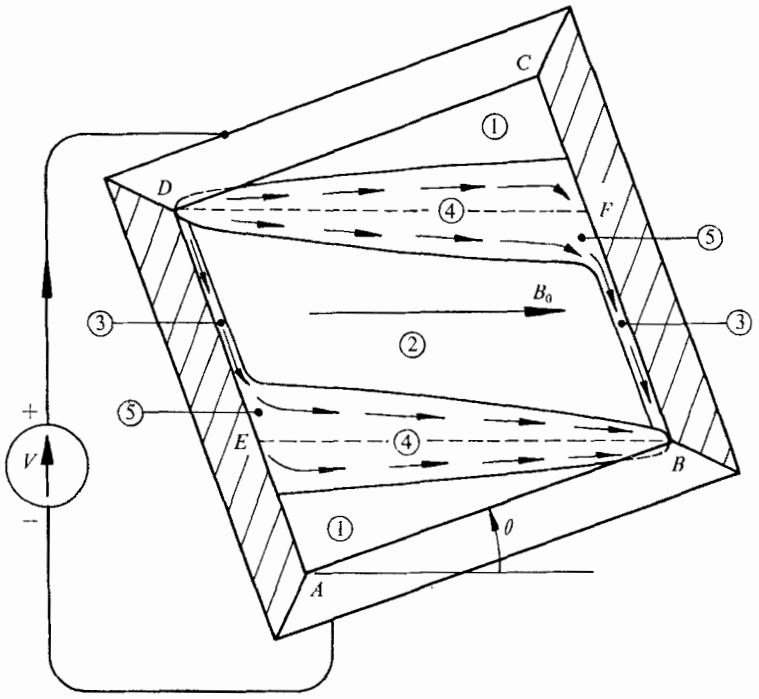

FIGURE 4. Approximate current flow lines for the electrically driven case without axial pressure gradient for $\theta < 45°$ (drawn for the case of $\theta = 20°$ and $M = 200$). The thickness of the skew Hartmann boundary layers is exaggerated.

The two zones 3 are again skew Hartmann boundary layers of thickness of order $a/M\cos\theta$. In these layers the electric field vector changes from being in the directions DE and FB in the fluid at the walls to being perpendicular to the transverse magnetic field at the outer edges of the layers. The current density, which is in the directions DE and FB, has its maximum value at the walls and decreases exponentially to zero at the outer edges of the layers. It is everywhere of such a value that the resulting Lorentz forces balance the local viscous forces due to the variation of velocity.

The two zones 4 are again viscous layers of thickness of order $a/M^{\frac{1}{2}}$ lying parallel to the applied magnetic field within which the velocity varies in approximately the error function manner. The electric field varies from zero in the two zones 1 to its uniform value in the direction normal to the applied magnetic field in zone 2. Within the layers current flows predominantly in the directions DF and EB with a density which tends to zero towards the edges of the layers. The dispersion of the layers and of the current within them with increasing distance from the corners B and D is such that the small current density component j_y gives rise to Lorentz forces which everywhere balance the local viscous forces. The current content of each of the layers is equal to that of one of the skew Hartmann boundary layers. The validity of the error function solution is again subject to uncertainty owing to the influence of the corners B and D. The two zones 5 are again skew Hartmann boundary layers of varying strength.

When allowance is made for the velocity deficiency due to the skew Hartmann boundary layers, the following approximate result is found for the mean velocity of flow through the duct at high Hartmann numbers:

$$v_0 = \frac{V}{2aB_0 \cos\theta}\left[1 - \frac{1}{M\cos\theta}\right]. \tag{4.2}$$

A topic of interest in experimental work is the effect of orientation and field strength on the apparent conductance of unit length of the duct, defined as the current flowing between the electrodes per unit length of the duct divided by the applied potential difference. The ratio of the apparent conductance $G_{M,\theta}$ at a Hartmann number M and orientation θ to the conductance G_0 at $M = 0$ is given by

$$\frac{G_{M,\theta}}{G_0} = \frac{1}{M(\cos\theta - \sin\theta)}, \tag{4.3}$$

which shows that the apparent electrical resistance of the duct at a particular orientation between zero and 45° is directly proportional to the Hartmann number, provided it is large.

The electrically driven case without axial pressure gradient is an example of the magnetohydrodynamic phenomenon of current channelling, whereby in the absence of pressure gradients the velocity distribution is such that current flow is confined to the direction parallel to the applied magnetic field, except in regions of varying velocity gradient where viscous forces are present to balance the Lorentz forces due to the crossing of the magnetic field by the current. This channelling effect was noted by Braginskii (1960) and discussed by Moffatt (1964) and Hunt & Williams (1968).

The solution of the pressure-driven short-circuited case may be derived by superposition from that of the electrically driven case without axial pressure gradient. We consider the régime in which the potential difference V between the electrodes has been reversed and an appropriate pressure gradient keeps the fluid at rest. Current of uniform density $\sigma V/2a$ flows parallel to the insulating walls, and the required pressure gradient is given by

$$-\partial p/\partial z = (\sigma V/2a)B_0 \cos\theta. \tag{4.4}$$

This régime and the electrically driven case without pressure gradient, shown in figure 4, are both solutions to the same linear differential equations. It follows that the sum of these two régimes is a solution to the equations subject to boundary conditions which are the sum of those applying to the two régimes separately. In the resulting situation the velocity distribution is identical to that of the electrically driven case without axial pressure gradient (since the second régime is stationary), the electrodes are both at the same potential and there is an axial pressure gradient given by (4.4). This is evidently the pressure-driven short-circuited case, shown in figure 3. If we use (4.4) to substitute for V in the expressions for core velocity (4.1) and mean velocity (4.2) in the electrically driven case, we obtain the results found in § 3 for the pressure-driven short-circuited case.

5. Orientations between 45° and 90°: pressure-driven or electrically driven

Figure 5 shows the square duct at an orientation between 45° and 90° and defines the new (x, y) and (x_1, y_1) co-ordinate systems. The perfectly conducting electrodes AB and CD overlap in projection in the direction of the applied magnetic field. Exactly similar reasoning to that given in § 3 suggests that the fluid in the triangles is again at rest. In the pressure-driven short-circuited case the $\mathbf{j} \times \mathbf{B}$ forces in the triangles balance the pressure gradient. In the electrically driven case without axial pressure gradient the triangles are at uniform potential and current free.

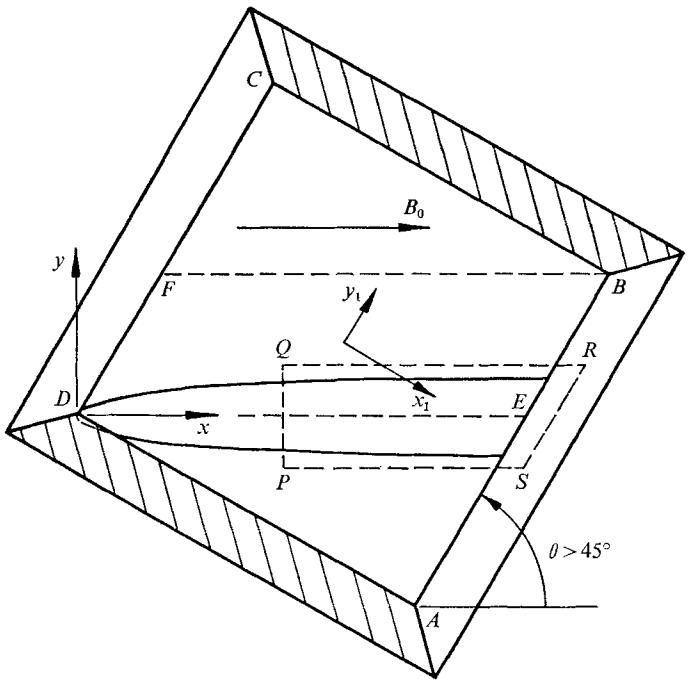

FIGURE 5. Cross-section of square duct for $\theta > 45°$, showing one of the shear layers.

On grounds similar to those given in §3 for the case of θ below 45°, we infer that in the central parallelogram region $EBFD$ the flow is the same as Hartmann flow between infinite plane perfectly conducting walls parallel to DF, with the same normal transverse magnetic field $B_0 \sin\theta$. If $M \sin\theta$ is large (where $M = B_0 a(\sigma/\eta)^{\frac{1}{2}}$ as before), the flow consists of a core of virtually uniform motion flanked by thin boundary layers of thickness of order $a/M \sin\theta$. We consider such a situation in which the flow is driven by a potential difference V between the perfectly conducting walls and an axial pressure gradient. Either driving agency may be put to zero to yield the pressure-driven short-circuited case or the electrically driven case without axial pressure gradient. We find the following results for the core of the flow:

$$\left.\begin{aligned} v_z &= (1/B_0^2\sigma)\,(-\partial p/\partial z) + V\cos\theta/2aB_0, \\ j_{x_1} &= -(\cos\theta/B_0)\,(-\partial p/\partial z) + \sigma V \sin^2\theta/2a, \\ j_{y_1} &= (\sin\theta/B_0)\,(-\partial p/\partial z) + \sigma V \sin\theta\cos\theta/2a. \end{aligned}\right\} \tag{5.1}$$

Applying these results to the square duct we find that in the electrically driven case without axial pressure gradient, shown in figure 6, the total current density in the core of region $EBFD$ is $\sigma V \sin\theta/2a$, parallel to the transverse magnetic field. This is another example of current channelling by a magnetic field. The total electric field in the core of the parallelogram is found to be $V/2a$ normal to the perfectly conducting walls.

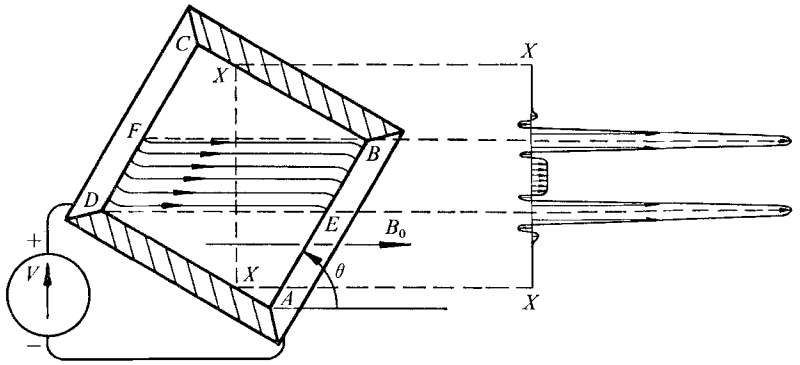

FIGURE 6. Approximate current flow lines and velocity profile for the electrically driven case without axial pressure gradient for $\theta > 45°$.

For the pressure-driven short-circuited case, figure 7, the total current density in the core of region $EBFD$ is $(1/B_0)\,(-\partial p/\partial z)$, perpendicular to the transverse magnetic field. It gives rise to Lorentz forces which balance the pressure gradient. E_{y_1} is zero everywhere, and from Ohm's law we find that E_{x_1} and, consequently, **E** are zero in the core of the parallelogram.

We now consider the régimes prevailing near to the lines DE and FB in figure 5. In both the electrically driven case without axial pressure gradient and the pressure-driven short-circuited case there are discontinuities across the lines DE and FB both in the velocity and in the component of electric field parallel to the applied magnetic field. The presence of these discontinuities suggests that in the electrically driven case there are thin shear layers, centred on the lines DE

and FB, resembling those discussed by Moffatt (1964), Waechter (1968) and Hunt & Stewartson (1969) in similar configurations. In the pressure-driven short-circuited case a pressure gradient and associated current flux across the layers are superimposed, but the flow structure is identical.

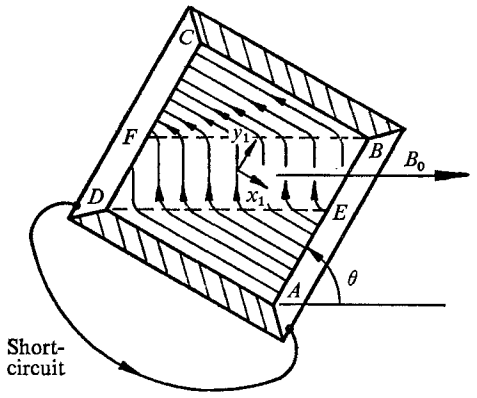

FIGURE 7. Approximate current flow lines for the pressure-driven short-circuited case for $\theta > 45°$.

We may, without exact analysis, determine the order of magnitude of the thickness of each layer and of the velocities occurring within it. We consider the electrically driven case. The y component of the Ohm's law equation for a point within the layer of thickness δ centred on DE in figure 5 is

$$j_{y\delta}/\sigma = E_{y\delta} + v_{z\delta} B_0, \tag{5.2}$$

where the suffix δ denotes a quantity within the layer. Applying the equation $\operatorname{div} \mathbf{j} = 0$ to the layer and assuming that j_x is of the same order in the layer as in the parallelogram, we find the approximate result $j_{y\delta} = O\ (\delta/a)\,(\sigma V \sin\theta/2a)$. Since in steady flow $\oint \mathbf{E}.d\mathbf{l}$ is zero around the path $PQRSP$, and $\mathbf{E}$ is zero along RS and SP, and E_x is of value $V \sin\theta/2a$ in the core of the parallelogram, we have $E_{y\delta} = O\ (a/\delta)\,(V \sin\theta/2a)$. Equation (5.2) then yields the result

$$v_{z\delta} = O\left[\frac{a}{\delta}\frac{V \sin\theta}{2aB_0}\right]. \tag{5.3}$$

The Navier–Stokes equation for the layer has the form

$$\eta\left(\frac{\partial^2 v_{z\delta}}{\partial x^2} + \frac{\partial^2 v_{z\delta}}{\partial y^2}\right) - j_{y\delta} B_0 = 0. \tag{5.4}$$

Neglecting $\partial^2/\partial x^2$ in comparison with $\partial^2/\partial y^2$ within the layer on the assumption that the layer is thin, and substituting for $v_{z\delta}$ and $j_{y\delta}$, we find that

$$\delta = O(a/M^{\frac{1}{2}}), \tag{5.5}$$

which confirms that for large Hartmann numbers the layers are indeed thin. Since the uniform core velocity in the parallelogram region is given by

$$v_{z_c} = V \cos\theta/2aB_0,$$

it then follows that $$\frac{v_{z\delta}}{v_{z_c}} = O(M^{\frac{1}{2}} \tan\theta), \tag{5.6}$$

which shows that large velocities occur within the layer. The velocity distribution across the duct is approximately as shown in figure 6.

An approximate expression for the total flow rate through the duct may be derived from the double integration over the cross-section of the duct of the x_1 component of the Ohm's law equation.

$$\int_{-a}^{a}\int_{-a}^{a} (j_{x_1}/\sigma)\, dx_1 dy_1 = \int_{-a}^{a}\int_{-a}^{a} E_{x_1} dx_1 dy_1 - B_0 \cos\theta \int_{-a}^{a}\int_{-a}^{a} v_z dx_1 dy_1. \tag{5.7}$$

For the electrically driven case without axial pressure gradient the sole contribution to the integral on the left-hand side arises from the uniform component in the parallelogram region. For all values of y_1, $j_{x_1} = \sigma V \sin^2\theta/2a$

$$\int_{-a}^{a} E_{x_1} dx_1 = V,$$

the electrode potential difference. The total flow rate Q is equal to

$$\int_{-a}^{a}\int_{-a}^{a} v_z dx_1 dy_1.$$

Equation (5.7) then yields the result

$$Q = (2aV/B_0)(\sin\theta + \cos\theta). \tag{5.8}$$

This expression is subject to relative errors of order $(M \sin\theta)^{-1}$ on account of the skew Hartmann boundary layers and of order $M^{-\frac{1}{2}}$ due to the shear layers.

The volumetric flow rate Q_c through the core of the parallelogram region is given by

$$Q_c = v_{z_c} \times \text{Area } EBFD = (2aV/B_0)\cos\theta(1 - \cot\theta). \tag{5.9}$$

On subtracting Q_c from the total flow rate Q, we obtain the flow rate $2Q_\delta$ through the two shear layers. Thus

$$2Q_\delta = 2aV/B_0 \sin\theta. \tag{5.10}$$

For all orientations between 45° and 90° most of the flow is carried by the layers: the proportion of the flow which is carried by the core has its maximum value of 17 % when $\theta = 67\frac{1}{2}°$.

As in the case of θ less than 45°, it is interesting to examine the effect of orientation and field strength on the apparent conductance of unit length of the duct. The ratio of the conductance $G_{M,\theta}$ at Hartmann number M and orientation θ to that at $M = 0$ is found to be

$$G_{M,\theta}/G_0 = \sin\theta(\sin\theta - \cos\theta). \tag{5.11}$$

This result is independent of the Hartmann number provided it is large. This contrasts with the case of θ less than 45°, where the conductance at a given orientation is inversely proportional to M because all the current has to flow along the skew Hartmann boundary layers on the insulating walls, as in figure 4.

To deduce the volumetric flow rate through the duct in the pressure-driven short-circuited case shown in figure 7, we again use the technique of the double integration of the Ohm's law equation, noting that both the triangles and the parallelogram contribute to the current integral and that, by virtue of the short-circuit connexion,

$$\int_{-a}^{a} E_{x_1} dx_1 = 0$$

for all values of y_1. The result is

$$Q = \frac{4a^2}{B_0^2 \sigma}\left(-\frac{\partial p}{\partial z}\right)(1+\tan\theta). \tag{5.12}$$

This expression is subject to the same relative errors as (5.8). The flow rate $2Q_\delta$ through the two shear layers is given by

$$2Q_\delta = \frac{4a^2}{B_0^2 \sigma}\left(-\frac{\partial p}{\partial z}\right)\operatorname{cosec}\theta \sec\theta. \tag{5.13}$$

The pressure-driven short-circuited régime may again be derived from the electrically driven case without axial pressure gradient, figure 6, by superposing an appropriate uniform current density parallel to the insulating walls.

6. Experimental aims and apparatus

Experiments were performed to test the theory developed above for the pressure-driven short-circuited situation for orientations between zero and 90° at large Hartmann numbers. The first aim was to investigate the relationship between the pressure gradient, the transverse magnetic field strength, the mean velocity of flow and the orientation of the duct to the field. The theory requires modification to allow for the imperfection of the short-circuit connexion between the electrodes in the experimental ducts. On the assumption that the electrodes themselves remain equipotential surfaces, which was reasonably valid in the experimental ducts, the approximate relationships between the pressure gradient and the mean velocity v_0 $(= Q/4a^2)$ take the following forms:
for $\theta < 45°$

$$-\frac{\partial p}{\partial z} = \frac{B_0^2 \sigma v_0 \cos^2\theta}{(1+\sigma/G_c)\left[1-\frac{1}{M}\left(\sec\theta+\frac{\sigma/G_c}{\cos\theta-\sin\theta}\right)\right]}, \tag{6.1}$$

and for $45° < \theta < 90°$

$$-\frac{\partial p}{\partial z} = \frac{B_0^2 \sigma v_0}{(1+\sigma/G_c)(1+\tan\theta)}, \tag{6.2}$$

in which G_c denotes the conductance of the external circuit per unit length of duct. Equation (6.1) obviously fails when θ is very close to 45°. For the case of zero orientation with an imperfect short-circuit the following relationship may be deduced from the work of Hunt & Stewartson (1965):

$$-\frac{\partial p}{\partial z} = \frac{B_0^2 \sigma v_0}{(1+\sigma/G_c)\left[1-(1+\sigma/G_c)/M - O(M^{-\frac{3}{2}})\ldots\right]}. \tag{6.3}$$

The expressions (6.1) and (6.3) are consistent when $\theta = 0$ for large values of M. When $\theta = 90°$, no current flows in the short-circuit connexion and the following approximate expression derived from Hunt's (1965) analysis requires no alteration:

$$-\frac{\partial p}{\partial z} = \frac{B_0^2 \sigma v_0}{1 + 0{\cdot}3M^{\frac{1}{2}}}. \tag{6.4}$$

The second aim was to gain more direct information about the régimes within the duct by observing the potential distribution on one of the insulating walls.

Mercury was chosen as the working fluid and two experimental ducts designed. To achieve a continuous highly-conducting interconnexion between the electrodes, each duct was machined from solid round copper bar. The outside diameter was limited by the magnet gap of $1\frac{1}{2}$ in. The choice of the size of the square channel within the copper involved a compromise between increase in the Hartmann number and increase in the conductance of the 'short-circuit' connexion. As has been shown experimentally by Baylis (private communication), the layer of amalgam which forms on a copper surface exposed to mercury leads to extremely low contact resistance at the interface. The assertion by Glaberson, Donnelly & Roberts (1968) that copper would be dissolved by mercury at a prohibitive rate is false.

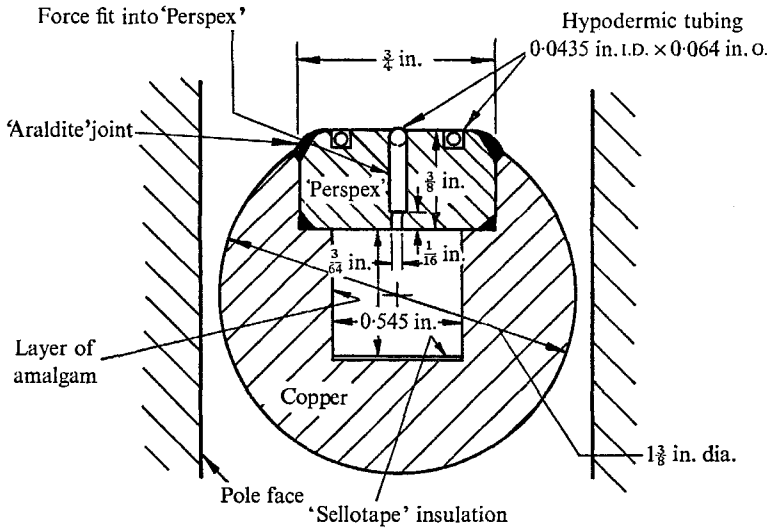

FIGURE 8. Transverse section of the ½ in. duct in position in the magnet gap.

In the first duct, shown in cross-section in figure 8, the flow channel was about ½ in. square by 15 in. long. The maximum attainable Hartmann number was about 230, while the conductance of the copper per unit length of duct was about 15 times that of the mercury. The bottom of the channel was insulated with a layer of 'Sellotape' adhesive tape. Six flush pressure tappings were located at 2 in. spacing along the centreline of the 'Perspex' cover. One of the tappings was also used for potential observations. The cover was fixed in place with 'Araldite' adhesive, but a succession of slow leaks occurred at the joints.

The second duct, shown in figures 9 and 10, incorporated an improved method of sealing the cover and additional flush tappings for the observation of potential at a series of positions across one insulating wall. The side of the square channel was about $\frac{3}{8}$ in.: the maximum attainable Hartmann number was 159, and the ratio of the conductance of the copper to that of the mercury was 21·8. The channel milled out of the copper ended 1 in. beyond the edges of the magnet poles, and the mercury flowed in and out through $\frac{1}{4}$ in. diameter axial bores from the ends. The channel was closed with a 'Tufnol' cover, sealed to the copper with a continuous 'O'-ring. Throughout the tests no leakage occurred at the seal. As shown in figure 9, the cover carried five equally spaced pressure tappings, P_1 to P_5, along its centreline, and five potential tappings, V_1 to V_5, all of $\frac{1}{32}$ in. bore.

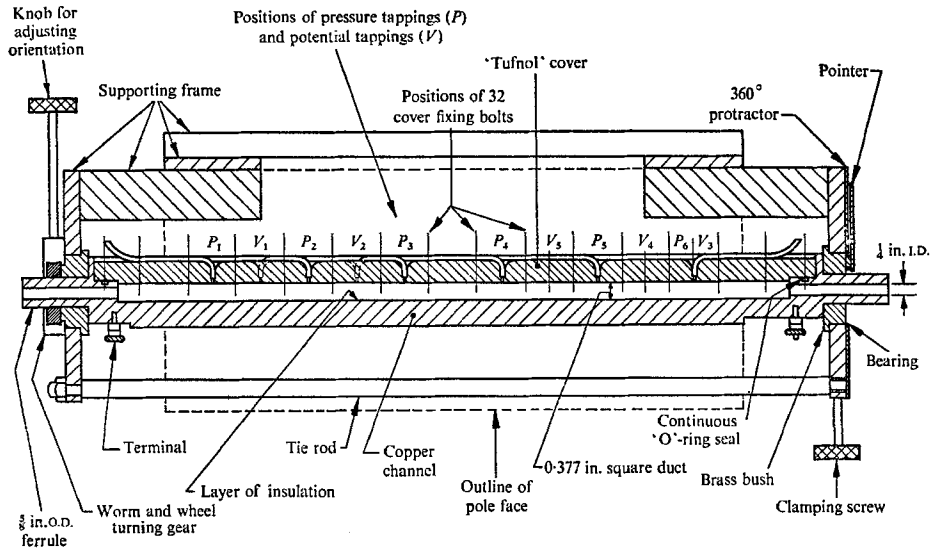

FIGURE 9. Axial section of the $\frac{3}{8}$ in. duct and the supporting frame.

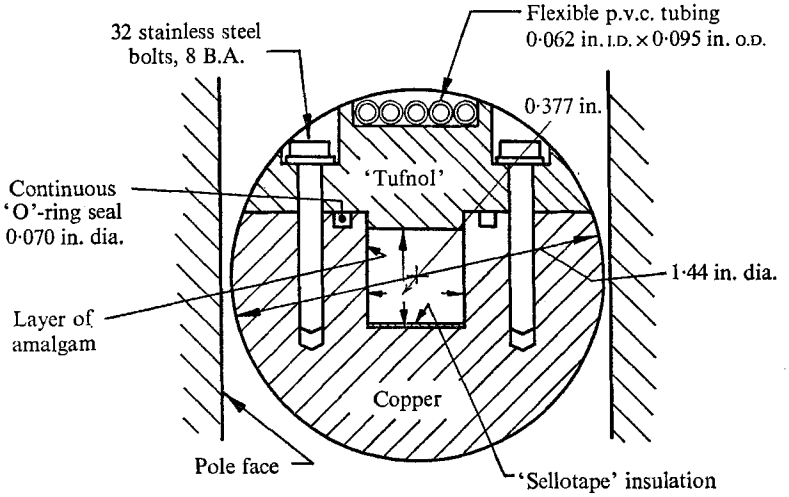

FIGURE 10. Transverse section of the $\frac{3}{8}$ in. duct in position in the magnet gap.

The electromagnet used in the experiments had a gap of $1\frac{1}{2}$ in. and rectangular pole faces measuring 12 in. by 5 in. The maximum attainable flux density at the centre of the gap was 1·27 webers/metre^2.

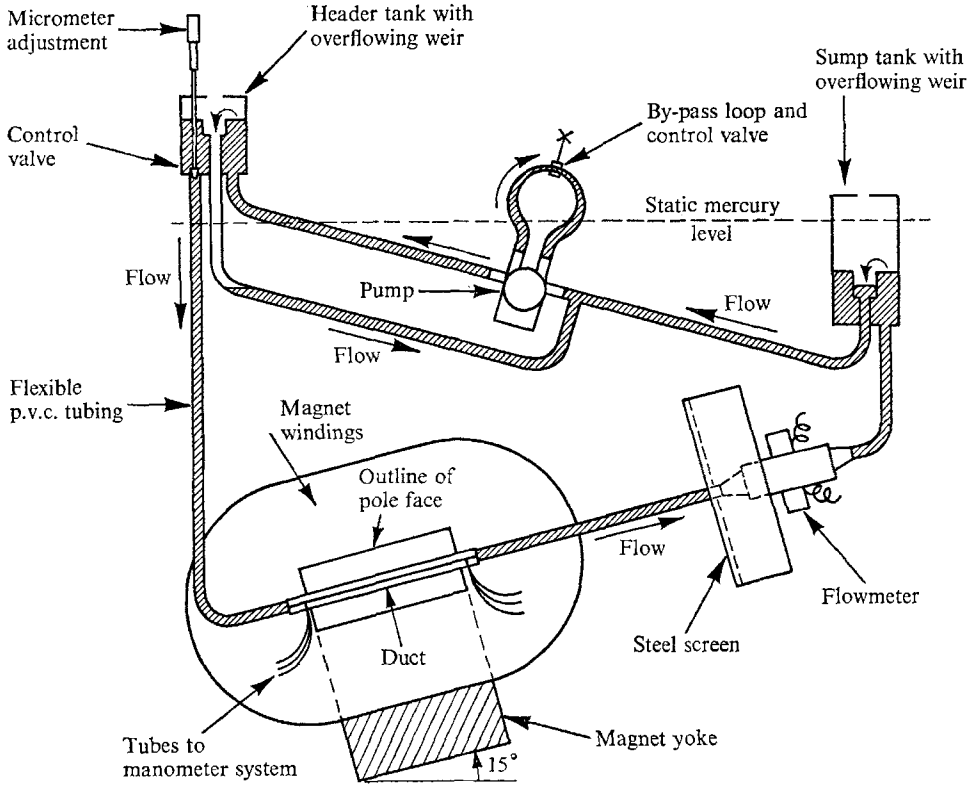

FIGURE 11. The mercury flow circuit. The magnet and tanks are shown in section.

The mercury flow circuit, shown in figure 11, incorporated a double weir, constant head system. The advantage of this arrangement over that described by Shercliff (1956) was that small fluctuations in the throughput of the pump would cause negligible changes in the mercury levels in the two Perspex tanks, so that very steady flow would prevail. The rate of overflow in the header tank was kept conveniently small by adjusting a by-pass loop around the pump. The use of p.v.c. tubing of $\frac{1}{2}$ in. bore and $\frac{1}{10}$ in. wall for the main pipework simplified the assembly and adjustment of the rig. The flow rate was indicated by a calibrated and screened electromagnetic flowmeter. Pressure differences were measured with a conventional two-fluid inclined tube manometer, using methylated spirits over mercury.

Full details of the apparatus and experiments are given by Alty (1966).

7. ½ in. duct: observations

The axial variation of pressure gradient, due to entry effects and non-uniformity of the magnetic field, was investigated with the ½ in. duct at zero orientation and a Hartmann number of 214 in tests at a succession of Reynolds numbers Re_a (based on the mean velocity v_0 and the half-width a of the duct) up to 2600. Even at the highest flow rate the pressure gradient measured between successive pairs of tappings was sensibly uniform along the duct, suggesting that the flow régime established itself very rapidly on entering the magnetic field. The observed pressure gradients were consistently a few percent higher than (6.3) predicts. In the subsequent tests with the ½ in. duct the pressure gradient was measured between the first and sixth tappings, located respectively 2 and 22 duct widths downstream of the entry into the magnet gap.

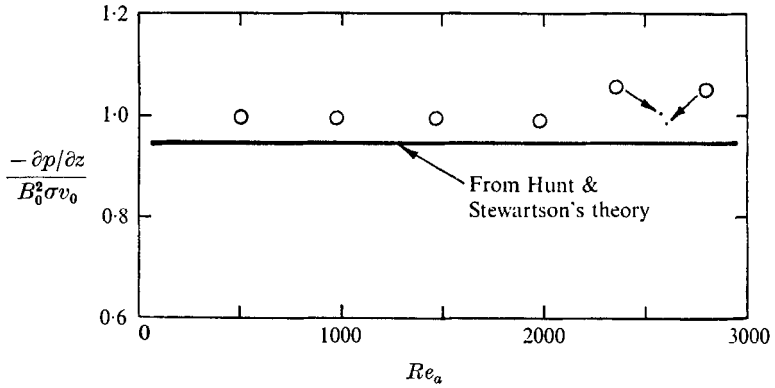

FIGURE 12. Graph of non-dimensional pressure gradient against Reynolds number ($Re_a = \rho v_0 a/\eta$) for the ½ in. duct at $\theta \sim 0$, $M = 228$. The straight line represents the approximate expression

$$\frac{-\partial p/\partial z}{B_0^2\sigma v_0} = \left[(1+\sigma/G_c)\left(1-\frac{1+\sigma/G_c}{M}\right)\right]^{-1},$$

derived from Hunt & Stewartson's (1965) theory.

Tests were made at a Hartmann number of 228 to reveal the variation of pressure gradient with flow rate at zero orientation. In figure 12 the results are plotted non-dimensionally and compared with Hunt & Stewartson's theory, using an estimated value of 0·065 for σ/G_c for the ½ in. duct. The results are consistently about 5 % higher than predicted.

In tests at orientations of $+89°$ and $-91°$, observations were made of the variation with flow rate of the pressure gradient and of the potential difference $\Delta\phi$ between the mercury at the mid-point of the insulating cover and the electrodes. $\Delta\phi$ was measured between one of the pressure tappings and a terminal on the axis of symmetry of the cross-section of the copper duct. The terminal would be at the (average) electrode potential since at this orientation the short-circuit connexion carries no current. The Hartmann number was 227 and the Reynolds number ranged from about 1000 to about 7000. Positive and negative orientations were used to reveal any possible asymmetry in the duct or magnetic field.

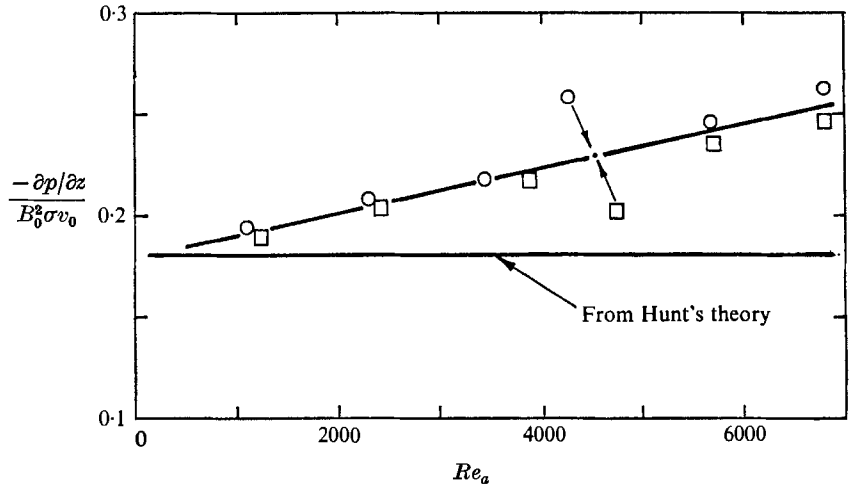

FIGURE 13. Graph of non-dimensional pressure gradient against Reynolds number for the $\frac{1}{2}$ in. duct at $\theta \sim \pm 90°$, $M = 227$. The straight line represents the approximate expression $(-\partial p/\partial z)/B_0^2\sigma v_0 = [1+0{\cdot}3\,M^{\frac{1}{2}}]^{-1}$, derived from Hunt's (1965) theory. ○, $\theta = 89°$; □, $\theta = -91°$.

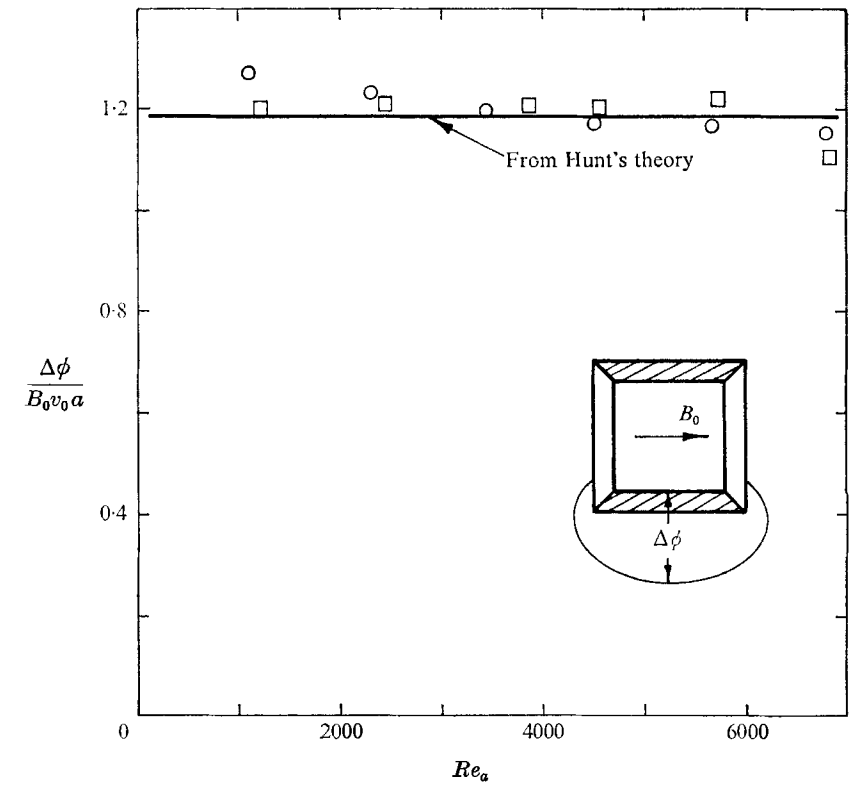

FIGURE 14. Graph of non-dimensional potential difference between the mid-point of one insulating wall and the electrodes against Reynolds number for the $\frac{1}{2}$ in. duct at $\theta \sim \pm 90°$, $M = 227$. The straight line represents the approximate expression

$$\Delta\phi/B_0 v_0 a = 0{\cdot}434[0{\cdot}3 + M^{-\frac{1}{2}}]^{-1},$$

derived from Hunt's (1965) theory. ○, $\theta = 89°$; □, $\theta = -91°$.

The results are plotted non-dimensionally and compared with Hunt's theory in figures 13 and 14.

Figure 13 shows that the observed pressure gradient agrees closely with Hunt's theory at low Reynolds numbers, but at higher flow rates exceeds the theoretical prediction by a factor which increases with Reynolds number, reaching a value of about 1·4 at $Re_a = 7000$. The discrepancy between the results for positive and negative orientations at the higher Reynolds numbers is insignificant since at these flow rates the pressure gradient and flow rate fluctuated erratically. The observations were made in relatively tranquil periods. By contrast, the potential observations taken during the same runs showed no major deviations from Hunt's theory. In figure 14 the discrepancies at the lowest and highest flow rates may be attributed to experimental error.

Since the entry length associated with Hunt's peaked velocity distribution is probably many duct widths in the present range of Reynolds numbers, it is highly likely that the duct length over which the average pressure gradients were observed included a region of developing flow. The large average pressure gradients observed would then be the result of enhanced currents circulating in the mercury in the settling region. The increase in settling length with flow rate would account for the divergence between experiment and theory with increasing Reynolds number. The close agreement in the case of the potential observations suggests that at the cross-section at which the potential measurements were made the flow régime resembled that predicted by Hunt, even at the higher Reynolds numbers. Hunt (1967) made direct measurements of the velocity profiles, using probes, which also indicated that the theory was qualitatively correct.

The fluctuations observed at the higher flow rates suggest that at some position along the duct certain regions of the flow, probably the developing high velocity boundary layers, became unstable. Such instability is not surprising in view of the contorted shape predicted by Hunt for the velocity profile in the boundary layer on each insulating wall. The continuity of the results suggests that there was not a sudden onset of instability throughout the flow but rather that, as might be expected, the turbulence originating in the boundary layers propagated only very slowly into the developing core of uniform motion. Thus it would have only a minor effect on the circulating currents and on the associated pressure gradient and wall potential.

8. $\frac{3}{8}$ in. duct: pressure gradient observations

When the $\frac{1}{2}$ in. duct developed leaks, the work was continued with the $\frac{3}{8}$ in. duct. Observations were made of the variation of pressure gradient with orientation at three constant Reynolds numbers, approximately 1000, 2900 and 4440, at each of two Hartmann numbers, 120 and 159. The pressure gradient was measured between tappings P_2 and P_5, located respectively 8 and 24 duct widths downstream of the entry into the magnet gap, as shown in figure 9. Typical results appear in non-dimensional form in figures 15(*a*) and (*b*). The theoretical curve for the Hartmann number of 120, using the experimentally determined value of 0·046

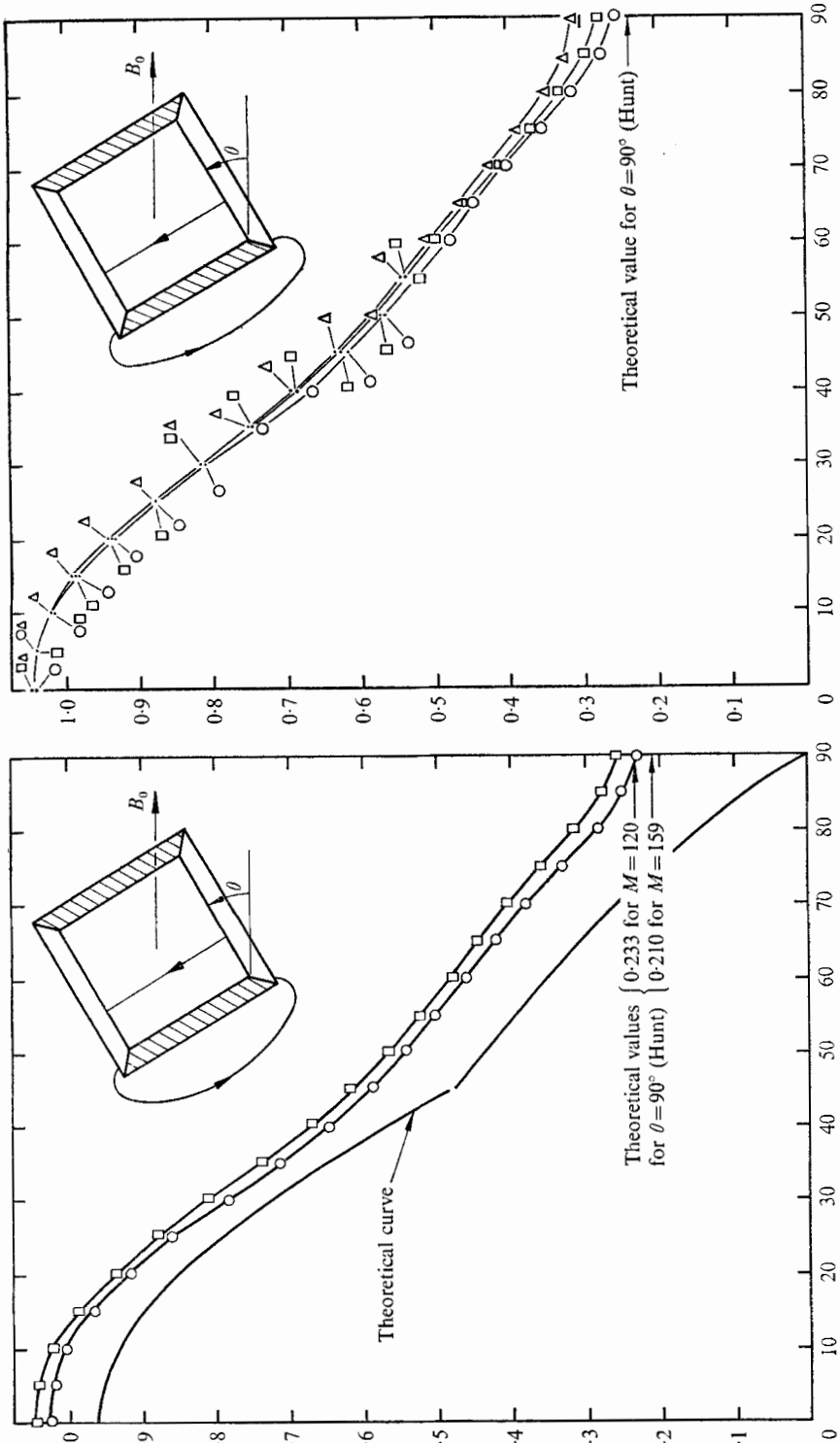

FIGURE 15. Graphs of non-dimensional pressure gradient against orientation for the ⅜ in. duct.
(*a*) At $Re_a \sim 1000$ for: □, $M = 120$; ○, $M = 159$. The theoretical curve represents equation (6.1), with $M = 120$, and equation (6.2).
(*b*) At $M = 120$ for: ○, $Re_a \sim 1000$; □, $Re_a \sim 2900$; △, $Re_a \sim 4440$.

for the conductivity ratio σ/G_c, is included in figure 15(*a*). The theoretical curve for the Hartmann number of 159 would be about 0·2 % lower for orientations below 45° and unchanged for orientations above 45°. The values given by Hunt's expression (6.4) for $\theta = 90°$ are also shown.

In figure 15(*a*), for the constant Reynolds number of 1000, the discrepancy between theory and experiment remains closely constant at about 0·085 for $M = 120$ and 0·065 for $M = 159$ for orientations up to 35°. Between 50° and 70° the discrepancy is again almost constant, but at the increased value of about 0·13 for $M = 120$ and 0·11 for $M = 159$. The values at 90° exceed Hunt's predictions by about 10 %. The corresponding curves for the Reynolds numbers of 2900 and 4440 are similar, showing the same constant vertical separation of about 0·02 between the curves for the Hartmann numbers of 120 and 159 for all orientations. Figure 15(*b*) shows that at the constant Hartmann number of 120 the non-dimensional pressure gradient is insensitive to Reynolds number for orientations up to about 30°, but thereafter increases with Reynolds number at a rate which itself increases with orientation.

Thus for orientations up to about 30° the non-dimensional pressure gradient exceeds the theoretical by an amount which depends on the Hartmann number but is almost independent of both orientation and Reynolds number. The discrepancies observed suggest a correction of order M^{-1} to the expression (6.1). The results obtained with the $\frac{1}{2}$ in. duct at zero orientation, which showed a discrepancy of 0·05 at $M = 228$, are consistent with such a correction.

9. $\frac{3}{8}$ in. duct: potential observations

The theory described in §§ 3 and 5 predicts a distribution of electric potential along either insulating wall which, unlike the pressure gradient, is crucially dependent on the velocity distribution over the cross-section of the duct. To throw light on the flow profiles, without the use of probes, observations were therefore made of the potential distribution along one insulating wall for a range of orientations of the duct.

For orientations below 45° we refer to figure 1. The theory indicates that the potential profile along AD closely resembles that which would prevail if the viscous layers centred on BE and DF were lines of discontinuity. In this 'bounding' profile the potential falls linearly from zero at A to the value

$$-V_0 = -(2a \tan\theta \sec\theta/B_0\sigma)(-\partial p/\partial z)$$

at E and then rises linearly to zero at D. The actual potential profile is rounded in the vicinity of E, in accordance with (3.13), owing to the finite thickness of the viscous layer centred on BE.

For orientations above 45° we refer to figure 7. The theory indicates that in the bounding profile the potential falls linearly from zero at A to the value

$$-V_0 = -(2a \sec\theta/B_0\sigma)(-\partial p/\partial z)$$

at D and then rises abruptly across the shear layer centred on DE to satisfy the short-circuit condition. The actual potential profile is rounded in the vicinity of D.

For each orientation we may non-dimensionalize the potential with respect to the peak potential difference V_0 of the bounding profile, and make allowance for the imperfection of the short-circuit connexion. We find that for orientations below 45° the non-dimensional bounding potential profile along the wall AD falls linearly from $-\sigma/2G_c \tan\theta$ at A to $-1-\sigma/2G_c \tan\theta$ at E and then rises linearly to $+\sigma/2G_c \tan\theta$ at D. For orientations above 45° it falls linearly from

$$-(\sigma/2G_c)\cos\theta(\sin\theta+\cos\theta) \quad \text{at } A \text{ to} \quad -1-(\sigma/2G_c)\cos\theta(\sin\theta+\cos\theta)$$

close to D, and then rises discontinuously across the shear layer to

$$+(\sigma/2G_c)\cos\theta(\sin\theta+\cos\theta)$$

at D.

To minimize entry effects and instability, all the potential observations were made at the low Reynolds number of 800. The Hartmann number was held at the maximum attainable value of 159. Runs were made at orientations ranging from $-80°$ to $+90°$ in increments of 10°, together with runs at $\pm 45°$ and at 180° and a series of runs around zero orientation. In each run the p.d. was measured between a terminal screwed into the copper on the axis of symmetry of the cross-section of the duct and each in turn of the five potential tappings V_1 to V_5 of figure 9. In the case of the runs at zero and positive orientations the p.d.s between the terminal and the heads of a pair of the cover fixing bolts shown in figure 10 were measured to show the effect of the finite resistance of the copper duct. For each orientation the potential observations were non-dimensionalized with respect to the peak potential difference V_0 of the appropriate theoretical bounding potential profile for a perfectly short-circuited duct, using extrapolated experimental values of $\partial p/\partial z$.

The results for orientations of $\pm 10°$, $\pm 30°$, $\pm 45°$, $\pm 60°$ and $\pm 80°$ are shown in figures 16(*a*) to (*c*), together with the theoretical non-dimensional bounding potential profiles, constructed using the experimental value 0·046 for σ/G_c. The results for the other orientations conform with the trend. For each positive orientation the non-dimensional potentials (relative to the terminal) at the tappings V_1 to V_5 are plotted at the appropriate positions, marked 1 to 5, along the axis representing the wall AD. The theoretical potential profile along AD for a given negative orientation is identical to that for the corresponding positive orientation if the potential differences are reversed and the profile plotted in the reverse direction along AD. The results for negative orientations are plotted in this way at locations -1 to -5 in figures 16(*a*) to (*c*). Since the arrangement of the potential tappings in the cover was asymmetrical, the positive and negative orientations together gave ten distinct points on each potential profile.

Except for the case of $\pm 10°$, the potential profiles for orientations up to 45° conform closely to the theoretical profiles. In particular, the agreement along the part AE of the wall provides direct evidence that the mercury was virtually at rest in the corner regions.

The results for $\pm 10°$ indicate the failure of the theory as the orientation approaches zero. The approximately triangular potential profile predicted by the theory for any non-zero orientation is incompatible with the profile at zero

orientation, which is antisymmetric about the mid-point of AD. However, the observed potential gradient between A and E is consistent with the theory. This suggests that even at this small orientation there are stagnant regions in the corners.

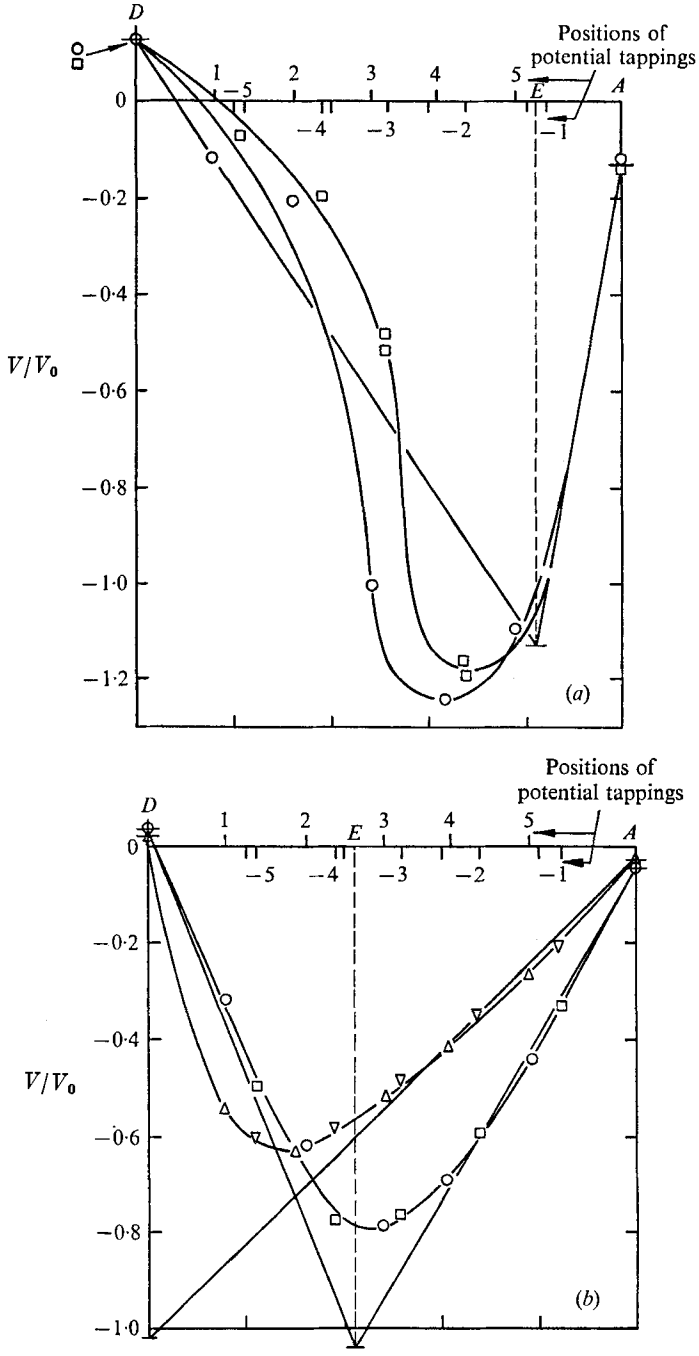

FIGURE 16. For legend see p. 457.

As the orientation rises from 45° to 80° the potential profiles depart increasingly from the theoretical bounding profiles. However, over the parts of the wall nearer to A the potential gradients do conform closely to the theory. This indicates that for these orientations there are again regions of stationary mercury in the corner A, but that with increasing orientation the shear layer emanating from D broadens progressively, with the result that the potential falls along a diminishing part of the wall AD and then rises gradually across the diffuse layer.

The profile for $\pm 80°$ shows the failure of the theory as the orientation approaches 90°. The potential profile departs from the skew distribution

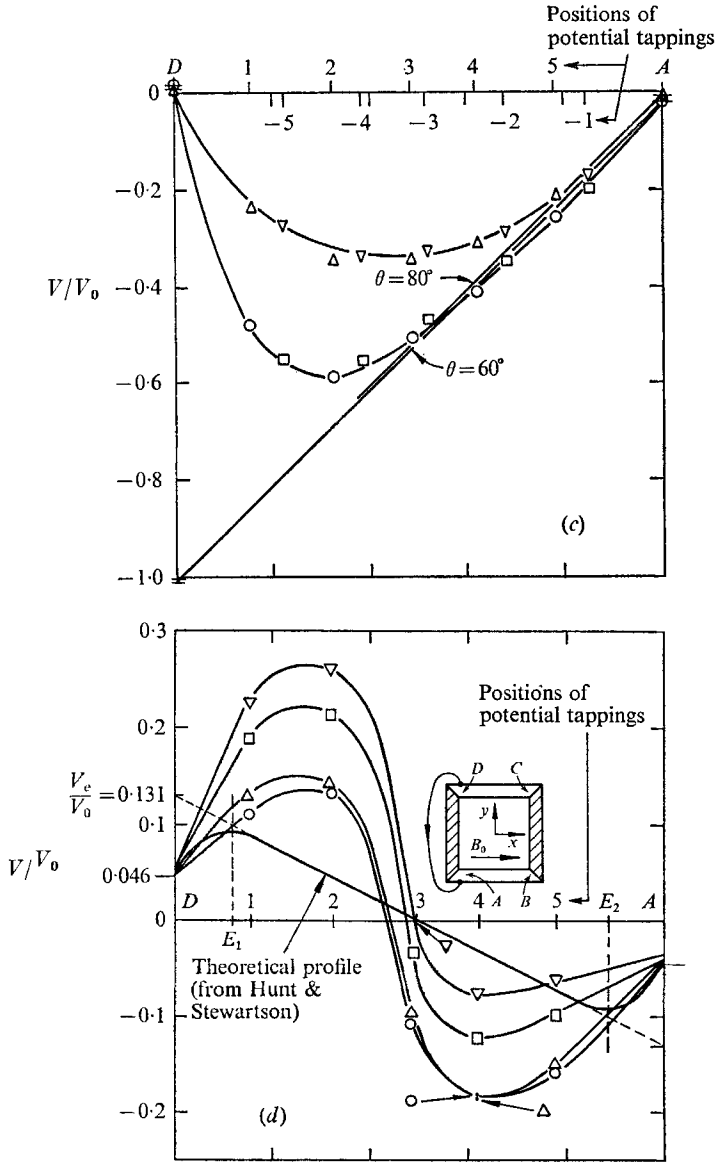

FIGURE 16. For legend see p. 457.

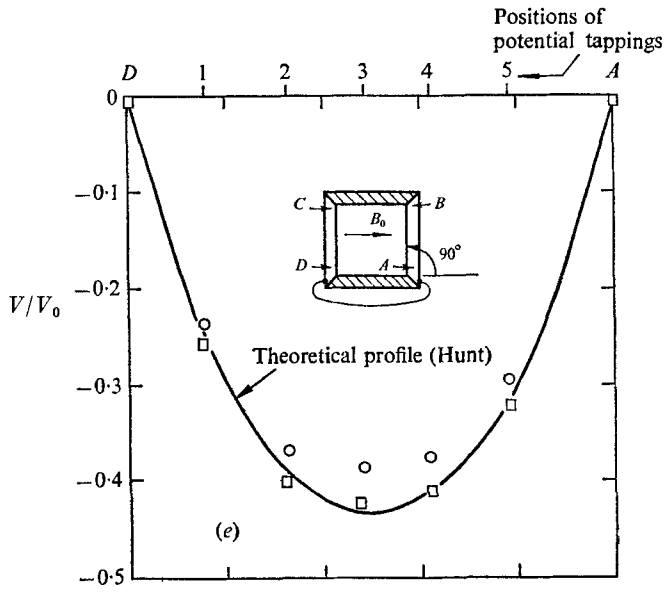

FIGURE 16. Non-dimensional potential profiles along the insulating wall AD for the $\frac{3}{8}$ in. duct for $M = 159$ and $Re_a \sim 800$, (*a*) ○, $\theta = +10°$; □, $\theta = -10°$: with theoretical bounding profile, modified to allow for the finite resistance of the current return path. Reference p.d. $= V_0 = (2a \tan\theta \sec\theta/B_0\sigma)(-\partial p/\partial z)$. (*b*) As (*a*) but: ○, $\theta = +30°$; □, $\theta = -30°$; △, $\theta = +45°$; ▽, $\theta = -45°$. (*c*) As (*a*) but: ○, $\theta = +60°$; □, $\theta = -60°$; △, $\theta = +80°$; ▽, $\theta = -80°$. Reference p.d. $= V_0 = (2a \sec\theta/B_0\sigma)(-\partial p/\partial z)$. (*d*) Orientations near to zero, with an approximate theoretical profile derived from Hunt & Stewartson (1965), allowing for the finite resistance of the current return path. Reference p.d. $= V_0 = (a/B_0\sigma)(-\partial p/\partial z)$. ○, $\theta = 0$; △, $\theta = -2°$; □, $\theta = -3\frac{1}{4}°$; ▽, $\theta = -4\frac{3}{4}°$. (*e*) $\theta = 90°$, with Hunt's (1965) theoretical profile. Reference p.d. $= V_0 = a^2(-\partial p/\partial z)/(M\sigma\eta)^{\frac{1}{2}}$. ○, V_0 based on experimental pressure gradient; □, V_0 based on theoretical pressure gradient.

predicted by the theory and approaches the symmetrical shape which it must take at 90°.

The results for a series of runs at orientations close to zero and 180° are given in figure 16(*d*). The observed potential differences were non-dimensionalized with respect to a reference p.d. V_0 given by $V_0 = (a/B_0\sigma)(-\partial p/\partial z)$, the appropriate value for the pressure gradient again being found by extrapolation from the earlier experimental results.

In figure 16(*d*) the curve for zero orientation is a mean profile derived from three complete series of observations. The profiles for zero orientation with the magnetic field reversed and for 180° are of similar form after reversal of sign. The skewness of the profile for zero orientation suggested that the duct was actually at a small positive orientation, but the profiles obtained from further runs at settings of $-2°$, $-3\frac{1}{4}°$, and $-4\frac{3}{4}°$ showed that at no setting would a symmetrical potential profile be obtained. The skewness was evidently due to some cause other than zero-error in orientation.

A theoretical potential profile along one insulating wall may be derived from Hunt & Stewartson's (1965) work. They derived a relationship between the core

velocity v_c and the mean velocity v_0, which is independent of the external circuit and for a square duct has the form

$$v_0 = v_c\left[1 - \frac{0{\cdot}956}{M^{\frac{1}{2}}} - \frac{1}{M} - O(M^{-\frac{3}{2}})\ldots\right]. \tag{9.1}$$

From (9.1) and the relationship (6.3) between pressure gradient and mean velocity for an imperfectly short-circuited square duct we have

$$v_c = \frac{1+\sigma/G_c}{B_0^2\sigma}\left(-\frac{\partial p}{\partial z}\right)\left[1 + \frac{0{\cdot}956}{M^{\frac{1}{2}}} + \left(0{\cdot}956^2 - \frac{\sigma}{G_c}\right)\frac{1}{M} + O(M^{-\frac{3}{2}})\ldots\right]. \tag{9.2}$$

Since the core current is given by $j_{y_c} = (1/B_0)(-\partial p/\partial z)$, it follows from Ohm's law that the electric field E_{y_c} in the core is given by

$$E_{y_c} = \frac{1-1}{B_0\sigma}\left(-\frac{\partial p}{\partial z}\right)\left\{\frac{\sigma}{G_c} + \left(1+\frac{\sigma}{G_c}\right)\left[\frac{0{\cdot}956}{M^{\frac{1}{2}}} + \left(0{\cdot}956^2 - \frac{\sigma}{G_c}\right)\frac{1}{M} + O(M^{-\frac{3}{2}})\ldots\right]\right\}. \tag{9.3}$$

Since E_y is independent of x except in the boundary layers on the electrodes, it follows that along the major part of the insulating walls the potential varies linearly, with the gradient given by (9.3). The straight line in figure 16 (*d*), cutting the potential axis at $V/V_0 = 0{\cdot}131$, represents this bounding potential profile, non-dimensionalized with respect to V_0.

Hunt & Stewartson's analysis shows that at a distance of $3a/M^{\frac{1}{2}}$ from the electrodes the velocity has risen to over 97 % of the core velocity. This distance, which we may regard as the theoretical boundary-layer thickness, is indicated by the points E_1 and E_2 in figure 16 (*d*). Within the boundary layers the non-dimensional potential would fall short of the bounding profile and vary smoothly towards the electrode non-dimensional potentials of $\pm\sigma/G_c$, approximately as shown.

Figure 16 (*d*) shows two major discrepancies between experiment and theory. First, the observed potential gradient over the central part of one insulating wall exceeds the theoretically predicted value by a factor of about 10. Secondly, the observed potential profiles, far from consisting of a linear central region flanked by thin boundary layers, show continuous non-linearity across the entire insulating wall.

A possible cause of the asymmetry of the profiles, but not of their unexpected magnitude, was the irregularity of the edge of the Sellotape strip forming the insulation on the wall of the duct opposite the Tufnol cover. Hunt & Stewartson showed that the effect of making the walls perpendicular to the magnetic field conducting over a length of order $a/M^{\frac{1}{2}}$ from the corners would be to reduce the potential difference across the boundary layer on each electrode. In the experimental duct this effect would occur near the Sellotape strip and gradually diminish towards the Tufnol wall, where the potential profile would be distorted and slightly flattened, but not steepened.

The form of the potential profiles has implications for the velocity distribution. The observed profiles can be approximately described by the equation

$$V = (0{\cdot}15a/B_0\sigma)(-\partial p/\partial z)\sin(\pi y/a).$$

If the current j_y is taken to be uniform at the value $(1/B_0)(-\partial p/\partial z)$ in the core of the flow, then Ohm's law indicates that the fluid velocity there is approximately given by

$$v_z = \frac{-\partial p/\partial z}{B_0^2 \sigma}[1 + 0{\cdot}5\cos(\pi y/a)]. \tag{9.4}$$

The viscous force per unit volume due to such a variation of velocity would be of order $M^{-2}(-\partial p/\partial z)$, which for large Hartmann numbers is small compared with $-\partial p/\partial z$. This result is consistent with the assumed value for j_y in the core. The shapes of the experimental potential profiles and of the corresponding deduced velocity profile are not understood. As they conflict so fundamentally with the expected régime of a core and boundary layers it is important that further tests be made to clarify the situation.

In the tests at zero and positive orientations the potentials of the two cover fixing bolts, plotted non-dimensionally at A and D in figures 16 (a) to (d), agreed very closely with the theoretical values, which are shown by short lines across the potential axes at A and D. This agreement confirms the theoretical relationships between the pressure gradients and the total circulating currents.

For the orientation of 90° the observed potentials, non-dimensionalized as in Hunt's (1965) theoretical analysis by dividing by the reference potential difference given by $V_0 = a^2(-\partial p/\partial z)/(M\sigma\eta)^{\frac{1}{2}}$, are plotted in figure 16 (e). Hunt's profile for the potential distribution is also shown. The experimental points marked with circles were derived by using in the calculation of V_0 an extrapolated experimental value of the pressure gradient. The points marked with squares were deduced using for the pressure gradient the value predicted by Hunt's theory for the relevant flow rate and magnetic field: they give the potential distribution non-dimensionalized with respect to mean velocity. The results differ because even when extrapolated down to a Reynolds number of 800 the experimental pressure gradient at 90° exceeded Hunt's predictions. When non-dimensionalized with respect to mean velocity the experimental results agree with Hunt's theory to within about 4 %. This close agreement supports the results obtained with the $\frac{1}{2}$ in. duct and described in § 7. The current flow within the copper from B to A and from C to D accounts for the small negative potentials at A and D, measured at the bolt heads.

10. Conclusion

The experimental results described in this paper suggest that the approximate theoretical analysis developed for the flow in square ducts with walls of mixed conductivities at arbitrary orientation to a transverse magnetic field at high Hartmann numbers is substantially true. The continuous change in the régime as the orientation of the two electrodes to the magnetic field is increased from zero to 90° is indicated.

At general orientations from zero to about 30° the non-dimensional pressure gradient is found to exceed the theoretical by an amount which is almost independent of both Reynolds number and orientation but varies with Hartmann

number approximately as M^{-1}. Between 50° and 70° the discrepancy for low Reynolds numbers is again almost constant but at an increased value: for higher Reynolds numbers it increases with orientation. Over the entire range of orientations and for all Reynolds numbers used, there is a constant difference in the observed values of the non-dimensional pressure gradients for Hartmann numbers of 120 and 159. Further tests over a range of Hartmann numbers are needed to clarify this effect.

The observed potential profiles along one insulating wall for zero orientation are radically different from the theoretical profile deducible from the work of Hunt & Stewartson (1965), and further experimental investigation of this technologically most important case is necessary. For orientations below 45° the potential profiles agree reasonably with the theory. They tend to confirm the existence of uniform flow in the central parallelogram region, which is thought to be bounded along lines through the corners parallel to the magnetic field by viscous layers of thickness of order $a/M^{\frac{1}{2}}$ in which the velocity varies in approximately the error function manner: the fluid in the triangles is observed to be at rest. It is suggested that as the orientation approaches 45° the velocity in the shrinking parallelogram increases until the two viscous layers coalesce into a diffuse, high velocity jet sheet. With increasing orientation the sheet is thought to separate into two high velocity layers of thickness of order $a/M^{\frac{1}{2}}$ centred on the lines through the corners parallel to the magnetic field, with a region of slow uniform motion between them: the experiments again indicate that the fluid in the triangles is at rest. As the orientation increases towards 90° the two layers are thought to approach the insulating walls and become ultimately the high velocity boundary layers predicted by Hunt (1965).

The tests at 90° and at low Reynolds numbers gave results for the pressure gradient and for the potential distribution along one insulating wall which agree well with Hunt's (1965) analysis. At higher Reynolds numbers the pressure gradient exceeds Hunt's predictions by a factor which increases with Reynolds number. This result is thought to be due to entry effects. The potential at the mid-point of one insulating wall agrees closely with the theory up to the maximum attainable Reynolds number of about 7000.

The author is grateful to Professor J. A. Shercliff for suggesting this research project, and for his most valuable help and advice throughout the work and in the preparation of this paper. The experiments were done in the Cambridge University Engineering Laboratories, under a contract with the Harwell and Culham Laboratories of U.K.A.E.A., while the author was supported by a grant from the D.S.I.R. (later S.R.C.).

REFERENCES

ALTY, C. J. N. 1966 Ph.D. Thesis, Cambridge University.

BRAGINSKII, S. I. 1960 *Sov. Phys. J.E.T.P.* **10**, 1005.

GLABERSON, W. I., DONNELLY, R. J. & ROBERTS, P. H. 1968 *Phys. Fluids*, **11**, 2192.

HASIMOTO, H. 1960 *J. Fluid Mech.* **8**, 61.

HUNT, J. C. R. 1965 *J. Fluid Mech.* **21**, 577.

HUNT, J. C. R. 1967 Ph.D. Thesis, Cambridge University.

HUNT, J. C. R. & MALCOLM, D. G. 1968 *J. Fluid Mech.* **33**, 775.

HUNT, J. C. R. & STEWARTSON, K. 1965 *J. Fluid Mech.* **23**, 563.

HUNT, J. C. R. & STEWARTSON, K. 1969 *J. Fluid Mech.* **38**, 225.

HUNT, J. C. R. & WILLIAMS, W. E. 1968 *J. Fluid Mech.* **31**, 705.

KULIKOVSKII, A. G. 1968 *Izvest. Akad. Nauk S.S.S.R., Mekh. Zhidkosti Gaza* (Mechanics of Liquids and Gases), no. 2, 3–10.

MALCOLM, D. G. 1968 *Proc. 6th Symposium on Magnetohydrodynamics*, Riga, Latvia, U.S.S.R.

MOFFATT, H. K. 1964 *Proc. 11th Int. Cong. Appl. Mech.*, Munich, 946–953.

SHERCLIFF, J. A. 1953 *Proc. Camb. Phil. Soc.* **49**, 136.

SHERCLIFF, J. A. 1956 *J. Fluid Mech.* **1**, 644.

SHERCLIFF, J. A. 1965 *A Textbook of Magnetohydrodynamics*. Oxford: Pergamon.

SHERCLIFF, J. A. 1967 Lecture given at Institute of Mechanics, University of Moscow, U.S.S.R.

TODD, L. 1967 *J. Fluid Mech.* **28**, 371.

WAECHTER, R. T. 1968 *Proc. Camb. Phil. Soc.* **64**, 871.

YAKUBENKO, A. YE. 1963 *Zh. Prikl. Mekh. Tekh. Fiz.* no. 6, 7. NASA Transl. F-241, Sept. 1964.